ChemPhotoChem

Articles
doi.org/10.1002/cptc.202000168

Chem
Europ
European C
Societies P

Check for
updates

Hydrogen Bonding Optimizes Singlet Fission in Carboxylic Acid Functionalized Anthradithiophene Films

Melissa K. Gish,[a] Karl J. Thorley,[b] Sean R. Parkin,[b] John E. Anthony,[b] and Justin C. Johnson*[a]

The rate of singlet fission, the process of generating two triplet excitons with photoexcitation of one singlet exciton, depends on a combination of singlet/triplet energy balance and intermolecular coupling. Here, we perform carboxylic acid functionalization of anthradithiophene (ADT) derivatives that results in hydrogen bonds that drive molecular orientation and strong electronic coupling of polycrystalline ADT thin films, leading to ultrafast singlet fission without significant enthalpic driving force. ADT with a single carboxylic acid group exhibits weak intermolecular coupling and slow and inefficient singlet fission, much like the parent ADT, and substitution of different alkylsilyl solubilizing groups has little effect. However, the addition of two carboxylic acid groups on either end of the long axis favors significant coupling and crystallinity in as-deposited thin films that increase the effective singlet fission rate by roughly three orders of magnitude. The properties of the triplet pair, particularly its propensity to form long-lived independent triplets, are also influenced by the degree of long-range intermolecular coupling. The enhancement of intermolecular coupling specific to singlet fission using the ubiquitous cyclic hydrogen bonding motif could impact triplet pair utilization schemes in a variety of contexts.

1. Introduction

Singlet fission (SF) is an exciton multiplication process that transforms an excited singlet state into two lower energy triplets, thereby potentially producing two electron-hole pairs with one photon.[1] The use of SF molecules in photovoltaic cells represents one route for circumventing the theoretical Shockley-Queisser power conversion efficiency limit of 33% toward a limit of 45%.[2] Additionally, in dye-sensitized solar cell (DSSC) configurations, SF molecules at metal oxide interfaces could surpass the champion 14% efficiencies without the use of heavy metals.[3] However, there are many factors that contribute to the efficiencies and rates of SF, including, but not limited to, energetics, local molecular orientation, and crystallinity (i.e., long-range order). Controlling these parameters in a systematic way toward a specific outcome such as high singlet fission efficiency is a challenging ongoing area of research.

Singlet fission requires that the energy of the singlet state $(E(S_1))$ be similar to or larger than twice the energy of the triplet $(E(T_1))$, constituting a roughly isoergic or exoergic

$(E(S_1) \geq 2E(T_1))$ process.[1–3] The creation of two free triplets $(T_1 + T_1)$ via singlet fission occurs through an intermediate state, known as the correlated triplet pair, which initially maintains a net singlet spin $(^1(TT))$. Anthradithiophene (ADT) is a previously studied SF compound with some favorable photophysical properties.[4] Despite the reported energy balance between singlet and triplet pair suggesting that ADT undergoes exoergic SF, which is typically ultrafast, SF in ADT is slow, occurring on the time scale of hundreds of picoseconds through nanoseconds.[4b] A study of ADT dimers in solution suggests that precise control over the molecular orientation of neighboring chromophores in ADT is necessary to optimize the coupling matrix element between S_1 and $^1(TT)$.[4a] The slow SF in ADT films and the strong sensitivity to coupling in ADT dimers in solution calls into question the strong exothermicity suggested by previous work[5] and instead implies approximately isoergic or slightly endothermic SF, indicating that ADT may be more analogous to tetracene than pentacene.

While work on ADT dimers is illuminating, the accessible short- and long-range electronic coupling afforded by molecular crystals is advantageous for completing the SF process, including generation of independent triplets. Crystal engineering is a strategy for controlling SF at the molecular level; however, striking a balance between favorable intermolecular coupling and energetics in SF systems is difficult.[6] The herringbone crystal arrangement adopted by unsubstituted acenes is often cited as the ideal configuration for fast and efficient SF.[7] Recent computational studies by Buchanan and co-workers determined that, for tetracene, this is not necessarily the case;[8] instead finding optima in which tetracene molecules are displaced along all axes such that

[a] Dr. M. K. Gish, Dr. J. C. Johnson
Chemistry and Nanoscience Center
National Renewable Energy Laboratory
15013 Denver West Parkway, Golden, CO 80401 (USA)
E-mail: justin.johnson@nrel.gov
[b] Dr. K. J. Thorley, Dr. S. R. Parkin, Dr. J. E. Anthony
Department of Chemistry
University of Kentucky
Lexington, Kentucky, 40506 (USA)

ChemPhotoChem

Articles
doi.org/10.1002/cptc.202000168

**Chemistry
Europe**

European Chemical
Societies Publishing

spatial overlap is present between just one aromatic ring of each partner, and thus, maintaining minimally interacting charge densities. The detrimental effects of excessive inter-molecular coupling in tetracene have also been shown experimentally.[6b,9] These studies demonstrate that while moderate wavefunction overlap in endoergic systems improves the SF coupling, the endoergicity of the system also increases, significantly slowing SF. As SF in ADT might also be roughly isoergic, it is important to be aware of how small changes in intermolecular interactions can alter the SF dynamics.

In rare but noteworthy cases, endothermic SF proceeds efficiently and quickly, despite a large thermal barrier towards triplet formation.[6b,9] Those studies point out that the change in Gibbs free energy for SF contains both enthalpic and entropic contributions. A significant entropic contribution could explain efficient endothermic SF, a possibility recently explored both theoretically and experimentally.[9–10] Mechanistically, delocalization of the initially excited singlet state provides access to a number of microstates of localized correlated triplet pairs that are energetically similar. A larger delocalization radius means access to a greater number of triplet pair configurations, allowing endothermic SF to proceed spontaneously at room temperature. Recently, Korovina and co-workers demonstrated the effects of the exciton delocalization length on endothermic SF with covalently linked perylene oligomers.[11] While dimers did not exhibit evidence of species beyond short-lived ^{1}(TT), trimers and tetramers showed significant yields of long-lived triplets. The extended network created in the oligomeric system promotes the full completion of SF by providing various configurations that can serve to host effectively independent triplets.

It is common for simple steric hindrance and the influence of van der Waals interactions to be used in crystal engineering schemes,[12] and each has been employed to influence SF.[6b,d,13] For example, the use of triisobutyl silyl vs. triisopropyl silyl solubilizing groups enhances the initial rate

of (TT) formation in substituted pentacene chromophores.[6d] Manipulation of hydrogen bonds as supramolecular synthons to assist in molecular self-assembly is also widely used to engineer crystallization in small organic molecules, inorganic molecules, and polymers,[14] representing a stronger driving force than van der Waals interactions. Carboxylic acid functionalization in polymers produces several hydrogen bonding motifs, including cyclic and lateral arrangements (Scheme 1).[14e,f] For example, terephthalic acid forms an extended network through cyclic hydrogen bonds, which promote order when crystallized.[15] In this investigation, we study the relative effects on the rate of SF of van der Waals vs. hydrogen bonding via side group and carboxylic acid substitution of ADT derivatives. We find that, like tereph-thalic acid, the carboxylic acid functionalization on the long axis promotes cyclic hydrogen bonding between ADT molecules in a thin film configuration and forms an extended network that increases intermolecular interactions, thus revealing ADT as a top-performing SF chromophore despite its relatively poor performance in films produced from other derivatives.

The photophysical properties of three functionalized ADTs (Scheme 1) are studied: the monoacids (TIBS-ADT-COOH, **1**) and (TIPS-ADT-COOH, **3**) and the diacid (TIBS-ADT-diCOOH, **2**). Despite small changes to the molecular structure, we observe drastic differences in SF dynamics. Thin films of monoacid derivatives (**1** and **3**) do not exhibit SF as a dominant excited state relaxation channel, though thin films of **1** show small but noticeable enhancement over **3**. Films of the diacid, **2**, undergo ultrafast SF, which has not been previously observed in ADT derivatives.[4] The single carboxylic acid in **1** and **3** limits hydrogen bonding to just a pair of molecules, which does not create a favorable environment for SF. The ability to form a continuous network of hydrogen bonds in **2**, when deposited in thin films, drives molecular orientation and increases entropic contributions necessary for SF. Organizing molecules to produce fast SF without excessive exoergicity leads directly toward goals
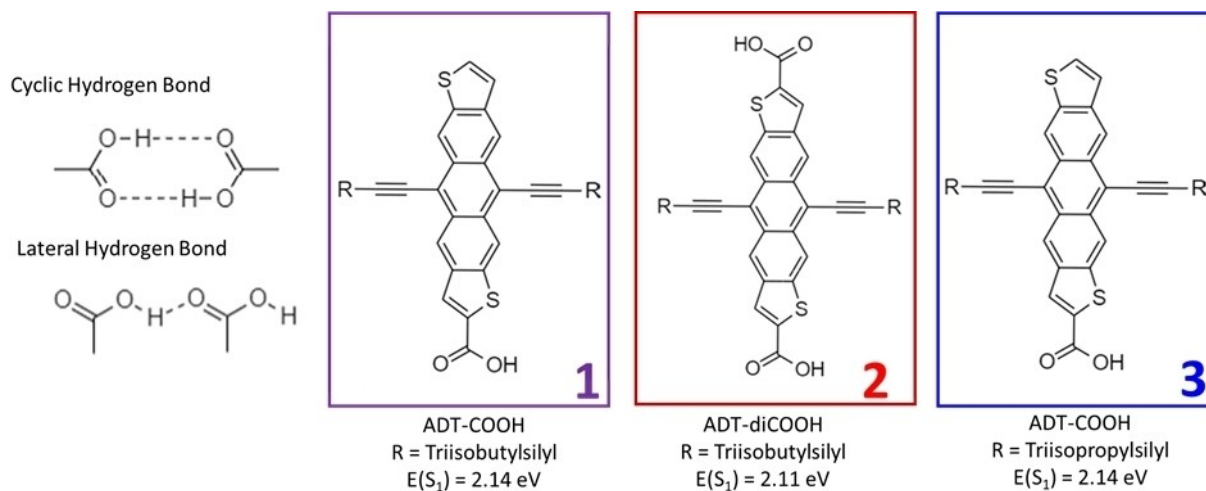
Scheme 1. Common hydrogen bonding motifs and chemical structures for TIBS-ADT-COOH (**1**),TIBS-ADT-diCOOH (**2**), and TIPS-ADT-COOH (**3**).

ChemPhotoChem

Articles
doi.org/10.1002/cptc.202000168

Chemistry Europe
European Chemical
Societies Publishing

inherent in solar energy conversion, which include the predominance of multiple triplet excited states with high electrochemical potential for charge transfer.

2. Results

The UV-Visible absorption spectra of **1**–**3** dissolved in THF (Figure 1A) exhibit vibronic structure typical of other acenes in solution, with a slight red shift of the absorption onset compared with tetracene.[3b,16] The spectrum of **2** is red shifted by about 15 nm with respect to **1** and **3**, which is expected with the addition of the second carboxylic acid group that withdraws electron density toward the periphery of the molecule. All compounds display a small Stokes' shift as observed by their emission profiles, and **2** emits at slightly lower energies than **1** and **3**. The singlet energy for the model compound TIBS-ADT in solution as determined by the crossing point of normalized absorption and fluorescence spectra is approximately 2.2 eV (Figure S1A). The singlet energies are 2.14 eV for **1** and **3**, and 2.11 eV for **2**, all lower than that of the model compound. The triplet energies for similar anthradithiophene derivatives have been determined to be ~1 eV[4b] suggesting singlet fission in these systems is roughly isoergic or slightly exoergic. Time-resolved photo-luminescence measurements reveal a fluorescence lifetime of 21 ns, 26 ns, and 27 ns for **1**, **2**, and **3**, respectively (Figure S1B, Table S1). The transient absorption spectra of the photoexcited singlet (Figure 1B) of **1**–**3** in solution contain similar features, though, like the steady state, **2** is red shifted from **1** and **3**. In both compounds, features include a broad photoinduced absorption (PIA) centered around 500 nm, a ground state bleach (GSB) at 525 and 576 nm for **1** and **3**, and 540 and 588 nm for **2**. The GSB peaks in the red region of the spectra are overlapping with stimulated emission, which also has minima at 622 and 680 nm, and 644 and 711 nm for **1** and **3**, and **2**, respectively. The triplet spectra of **1**–**3**, as determined by sensitization with anthracene, show peaks at 515 nm, 560 nm, and 615 nm for both, though the peak at 560 nm is more pronounced in **2**.

The absorption spectra of as-deposited (**AD**) thin films of **1**–**3** are shown in Figure 2. Deposition of **1** in a thin film gives rise to Davydov splitting, corresponding to a 32 nm shift in the 0-0 peak suggesting some degree of intermolecular coupling. The absorption spectrum of **2**-AD in a thin film exhibits a dramatic ~50 nm red shift in the 0-0 peak, as well as significant peak broadening, compared to solution. This is indicative of strong intermolecular coupling between the molecules in the thin film. The thin film spectrum of **3**-AD exhibits a small shift in the 0-0 peak position and little broadening compared with solution, pointing to minimal intermolecular interactions in this configuration. The emission of **1**–**3**-AD (Figure 2A) in films is much weaker than in solution, with red-shifted and broadened spectra. Solvent vapor annealing (SVA) of **2** (**2**-SVA, Figure S3A) increases the absorption red shift compared to the as-deposited film
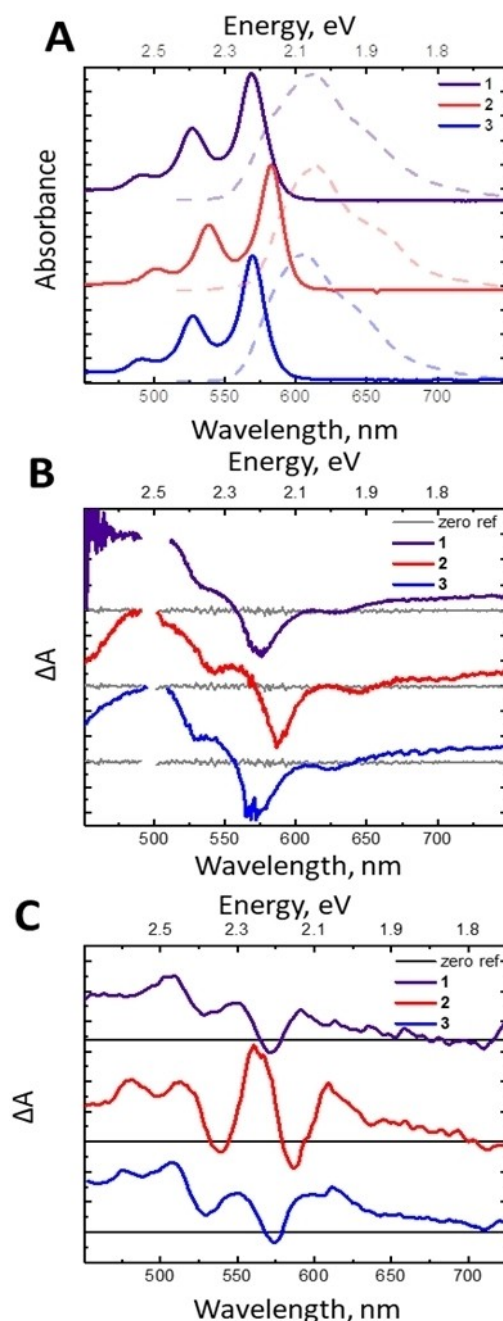

Figure 1. A) Normalized steady state absorption (solid) and emission (dashed) spectra of **1** (purple), **2** (red), and **3** (blue) in THF. B) Normalized transient absorption spectra in THF solution at 1 ps after 500 nm excitation (50 nJ/pulse). C) Normalized triplet spectra after sensitization with anthracene in THF solution as determined through global analysis. Spectra are offset for clarity.

consistent with a further increase in intermolecular coupling. Solvent vapor annealing of **3** under the same conditions shows no significant change in the absorption spectrum.

The XRD diffractograms of thin films of **1**–**3** are shown in Figure S4. The predicted powder pattern of **1** as determined from the experimental crystal structure displays similarities to the thin film pattern of **1**, which indicates a correlation between bulk and thin film crystalline phases. **1** shows some

ChemPhotoChem

Articles
doi.org/10.1002/cptc.202000168

Chemistry
Europe
European Chemical
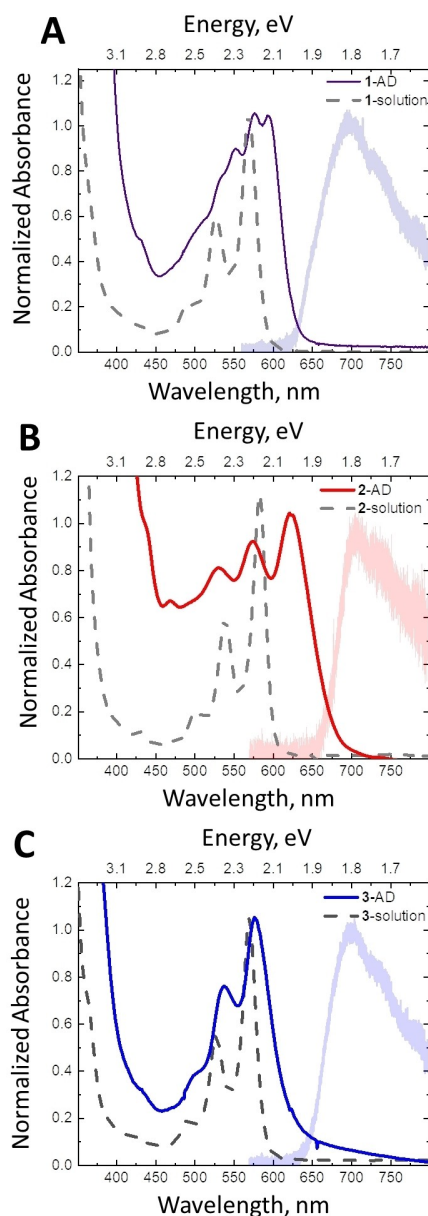Societies Publishing

Figure 2. A) Normalized steady state absorption and emission spectra of **1** in THF solution (dashed gray line), and as deposited (AD) in a thin film (purple). B) Normalized steady state absorption and emission spectra of **2** in THF solution (dashed gray line), and AD in a thin film (red). C) Normalized steady state absorption and emission spectra of **3** in THF solution (dashed gray line), and AD in a thin film (blue).

crystallinity as-cast (Figure S4A), and solvent or thermal annealing of **1** did not improve the long-range order and will not be discussed further. Contrastingly, as-deposited thin films of the other monoacid, **3** (Figure S4C), show a small peak at 5.4°, suggesting there is a minor amount of native crystallinity. After solvent vapor annealing, the peak at 5.4° significantly increases in amplitude, and sharp features at 10.6°, 12.5°, and 15.9° appear, indicative of a large increase in crystallinity of the thin film. XRD of **2** as-deposited (Figure S4B) reveals similar features to the solvent annealed film of **3** with the most prominent peak at 5.4°, as well as peaks at 10.6° and 15.9°. Solvent vapor annealing of **2**

increases the amplitude of these peaks slightly, but the patterns appear similar. We were unable to grow suitably large crystals of **2** for bulk crystal determination due to the interplay between van der Waals forces among side groups and strong hydrogen bonding interactions that frustrates extended crystal growth; therefore, we compared the thin film XRD diffractogram to the powdered material of **2**.[17]

Diffraction of the powdered material shows a variety of peaks, and a match with thin film peaks is detected, suggesting similar crystal structures for bulk and thin film but with considerable thin film texturing. Scherrer analysis for determination of average crystallite size, which is approximate but should provide a reasonable estimate,[18] indicates average sizes of 23, 25, and 49 nm for **1**, **2**, and **3**, respectively (Table S2).

Figure 3 shows the visible transient absorption spectra for as-deposited (AD) thin films of **1**–**3** after photoexcitation at 500 nm (35 nJ/pulse). Low pulse energies were used to isolate the dynamics of singlet fission by avoiding nonlinear effects, including singlet-singlet annihilation. The early time transient spectra of thin films of **1** after 500 nm photo-excitation are close to that of solution, with PIAs centered at 500 nm and 700 nm and GSB features at 550 and 600 nm (Figure 3A). The singlet features decay concomitant with a small rise of a positive feature at 580 nm that then begins to decay within the 5 ns window. The PIA at 580 nm is consistent with a triplet signature derived from solution sensitization experiments. Two species are derived from global analysis as shown in the species associated decay spectra (SADS) for **1** (Figure 3D). Here, it is clear that the initial species resembles the singlet ($S_0 S_1$) in solution (Figure 1B), while we assign the secondary species to the triplet state ($2(T_1)$).

Early time spectra of **3** (Figure 3C) are similar to that of **1**. Over the course of 5 ns, the PIAs in the blue and red regions of the spectra decay to about 25% of the original amplitude, and a small PIA feature is revealed consistent with the sensitized triplet signature. The spectrum at 5 ns contains signatures from both the singlet and triplet states, suggesting that singlet fission in as deposited films of **3** is slow and/or incomplete. The global analysis is unable to separate singlet and triplet features in the SADS of **3** (Figure 3F) confirming the inefficiency of free triplet formation in **3**. The TA spectra of a solvent annealed film of **3** (Figure S6A) look similar to the as-deposited film. The singlet PIA also decays to about 25% of its original amplitude, and the triplet feature is present with a similar prominence. Despite the apparent increase in crystallinity in the XRD pattern, the triplet feature remains small compared to the singlet features.

The transient behavior of thin films of the diacid, **2** (Figure 3B), is in stark contrast to that of monoacids, **1** and **3**. At 250 fs after photoexcitation at 500 nm (35 nJ/pulse), there is a sharp peak at 615 nm, assignable to the triplet, in addition to the PIAs at 500 nm and 700 nm. The position of the triplet compared to solution sensitization experiments is significantly red-shifted thus we performed a thin film
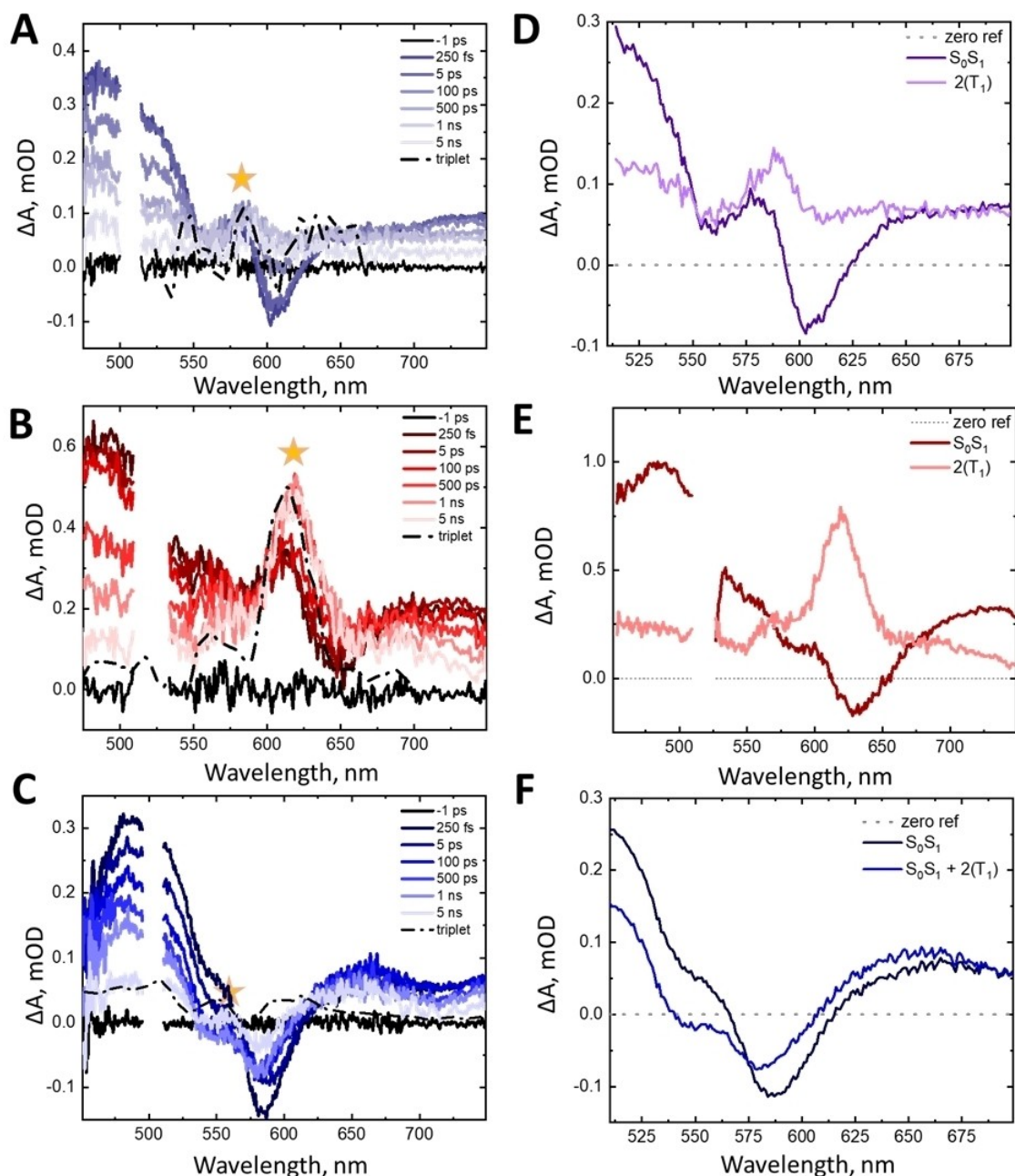
ChemPhotoChem

Articles
doi.org/10.1002/cptc.202000168

**Chemistry
Europe**
European Chemical
Societies Publishing

Figure 3. Transient absorption spectra of as-deposited thin films under a N_2 atmosphere excited at 500 nm (35 nJ/pulse) of **1** (A), **2** (B), and **3** (C) at pump-probe delays of −1 ps, 250 fs, 5 ps, 100 ps, 500 ps, 1 ns, and 5 ns with colors indicated by the legend. The dashed line represents the sensitized triplet derived from solution for **3**, and from thin film sensitization for **1** and **2**, and the star denotes the location of the triplet PIA of interest. The species associated decay spectra (SADS) are shown for **1** (D), **2** (E), and **3** (F).

sensitization of **2** to confirm our assignment (Figure S5A). The ratio of triplet to singlet PIA features at pump-probe delays within the instrument response time is already ~1:2 and becomes at least 5:1 as the singlet PIAs decrease with a time constant of 358 ps (Figure 4A, Table S2). The SADS of **2** (Figure 3E) reveals distinct species associated with S_0S_1 and 2 (T_1), consistent with solution measurements (Figure 1B) and thin film sensitization (Figure S5).

After solvent vapor annealing a thin film of **2** (Figure S6B), the ratio of triplet to singlet features at early pump-probe delays after photoexcitation is roughly 3:4, signifying

a 50% increase in the magnitude of the triplet signature. Additionally, the slow component becomes faster in the solvent vapor annealed film than the as-deposited film of **2**, decreasing from 358 ps to 155 ps (Figure 4, Table S3). Figure 4 shows a comparison of kinetic profiles, where the initial triplet amplitudes are normalized to the initial singlet population. Thin films of **1** exhibit a 66 ps rise in triplet signature; however, the magnitude of this increase is significantly less than that of **2**. The triplet concentration profiles derived from global analysis, displayed as solid lines in Figure 4, demonstrate the ultrafast rise in unannealed and
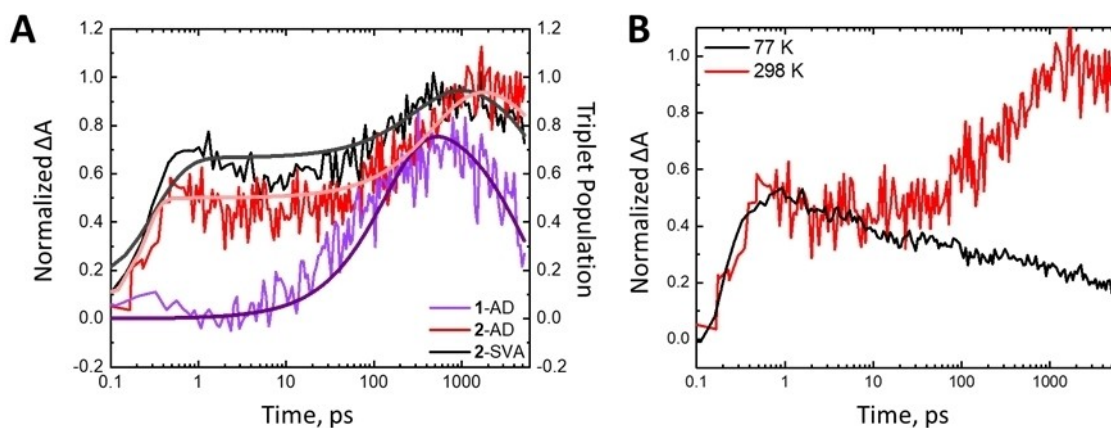
ChemPhotoChem

Articles
doi.org/10.1002/cptc.202000168

Chemistry
Europe
European Chemical
Societies Publishing

Figure 4. A) Normalized transient absorption kinetics probed at 615 nm after 500 nm photoexcitation of a thin film of as-deposited **1** (**1**-AD, purple), **2** (**2**-AD, red) and solvent vapor annealed **2** (**2**-SVA, black). Concentration profiles from global analysis are shown as solid lines. Fit parameters are found in Table S1 in the Supporting Information. The kinetics are normalized to the initial singlet population at 250 fs. B) Normalized transient absorption kinetics probed at 615 nm after 500 nm photoexcitation of a thin film of **2**-AD at 298 K (red) and 77 K (black).

annealed thin films of **2** that is not present in **1**. The subtle differences in kinetic traces and the concentration profiles are due to multiple overlapping features in the transient absorption spectra, particularly at early times. The triplet feature in thin films of **3** is barely observable above the noise, which makes it difficult to accurately determine a rise time. The near IR transient absorption data for films of **1** and **2** at room temperature (Figure S7A, Figure S8A, respectively) mirror the significant differences observed in the visible transient absorption. The spectra for as-deposited films of **1** (Figure S7A and B) are similar to the singlet spectrum in solution, including a broad PIA localized around 1250–1300 nm. There is a slow and subtle blue-shift of this PIA through 5 ns that further evolves to a defined peak centered at 925 nm. Measurements at 77 K reveal a sharper PIA, and the blue shift is slightly slowed, yet clearly evident (Figure S7D). The transient absorption of the as-deposited film of **2** at early pump-probe delays (Figure S8A and B) exhibits two distinct peaks centered at 1000 nm and 1150 nm. Between 500 ps and 5 ns, the two peaks decay into a single PIA centered ~975 nm. However, when **2** is probed at low temperatures, the two initially formed peaks persist through 5 ns without evolving into a single peak (Figure S8D–F). Thin films of **3**-AD do not have a significant temperature dependence in their kinetic behavior (Figure S10) but do undergo similar spectral changes as **1**-AD. Solvent vapor annealed thin films of **2** (**2**-SVA, Figure S9) also exhibit two distinct peaks similar to **2**-AD that decay into a singular peak at room temperature. At 77 K, evolution to the single peak is evident but slowed compared with room temperature. Based on thin film sensitization experiments (Figure S5B), we assign the peak at ~975 nm to separated triplets in thin films of **1**–**3**. Solution experiments indicate that the singlet appears at 1300 nm. This suggests the doubly peaked feature at 1150 nm and 1000 nm can be assigned to the correlated triplet pair (^{1}(TT)).

We also examined the temperature dependent TA in the visible spectral region for as-deposited thin films of **1** and **2**

(Figure S12). While the spectral features are independent of temperature, secondary growth of the triplet features seen for **2** at room temperature does not occur at 77 K (Figure 4B). Instead, the singlet decays to reveal a small triplet feature at long delays. Unlike the NIR region, where three separate species are present, the visible region only contains two distinct spectral features assignable to singlet and triplet transitions. The triplet lifetimes are drastically different among the films. Decay kinetics for **1-3** of the remaining features on time scales beyond 1 ns are shown in Figure 5A. The PIA for **1** and **3** at ~1000 nm decays with a time constant of 2.3 ns and 4.6 ns, respectively, while in **2**, this feature has a biexponential lifetime with a time constant of 1.7 ns, and a second lifetime of 135 ns (Table S4). The second component for **2** matches the decay of the triplet feature in the visible at 620 nm (Figure S14, Table S3). Solvent vapor annealing of **3** and **2** extends the lifetime to 34.1 ns and 599 ns, respectively (Figure S13).

Time correlated single photon counting (TCSPC) was utilized to detect prompt vs. delayed fluorescence signals, Figure 5B. The results of the multiexponential fits to the kinetics are in Table S5. After 450 nm excitation of **3** and probing at 690 nm, we observe a majority of the excited states decay back to baseline with a time constant of 17.7 ns. A small component of the decay appears to be instrument response limited suggesting a minority of the molecules are undergoing SF, consistent with the small triplet feature in the transient absorption spectra. The remainder of the long-lived luminescence resembles emission from isolated **3** in solution (Figure S1), although some small amount of delayed fluorescence due to triplet-triplet annihilation may be present. We observe a drastic difference in the behavior of **1** and **2**, where a fast initial decay is followed by a long tail with a time constant of ~30–35 ns (Table S4), longer than singlet decay of **1** and **2** in solution ($\tau_{S1} = 21$–26 ns). We assign this secondary decay to delayed fluorescence from triplet-triplet annihilation after singlet fission. This delayed component more than doubles in amplitude after annealing,
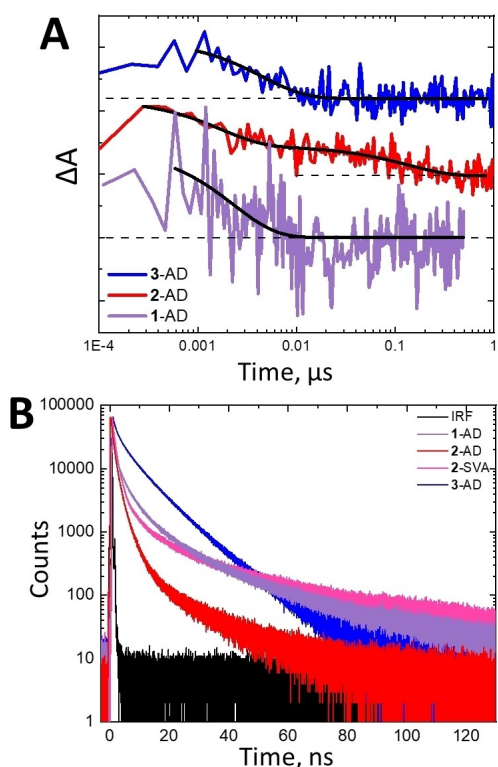
ChemPhotoChem

Articles
doi.org/10.1002/cptc.202000168

Chemistry Europe
European Chemical
Societies Publishing

Figure 5. A) Decay kinetics of as-deposited thin films of **1** (purple) and **2** (red), and **3** (blue) probed at 1000 nm after 500 nm photoexcitation. Kinetic traces are offset for clarity. Fits are shown as black lines and fit parameters are shown in Table S2. B) Time-correlated single photon counting (TCSPC) data for thin films of **1** (purple), **2** as deposited (red), **3** (blue), and solvent vapor annealed **2** (pink) excited at 450 nm and probed at 690 nm. Instrument response (IRF) is shown in black.

consistent with more efficient SF in annealed films of **2** (Figure 5B).

The calculated triplet yields (Table S6), although very uncertain due to experimental complexities, were determined for **2**-AD and **1**-AD and found to be near or exceeding 100%. We note that although the maximum triplet yields, representing the peak triplet population for a given compound, are similar for **1** and **2**, the yield of ultrafast triplets and very long-lived triplets is much larger for **2** than **1**.
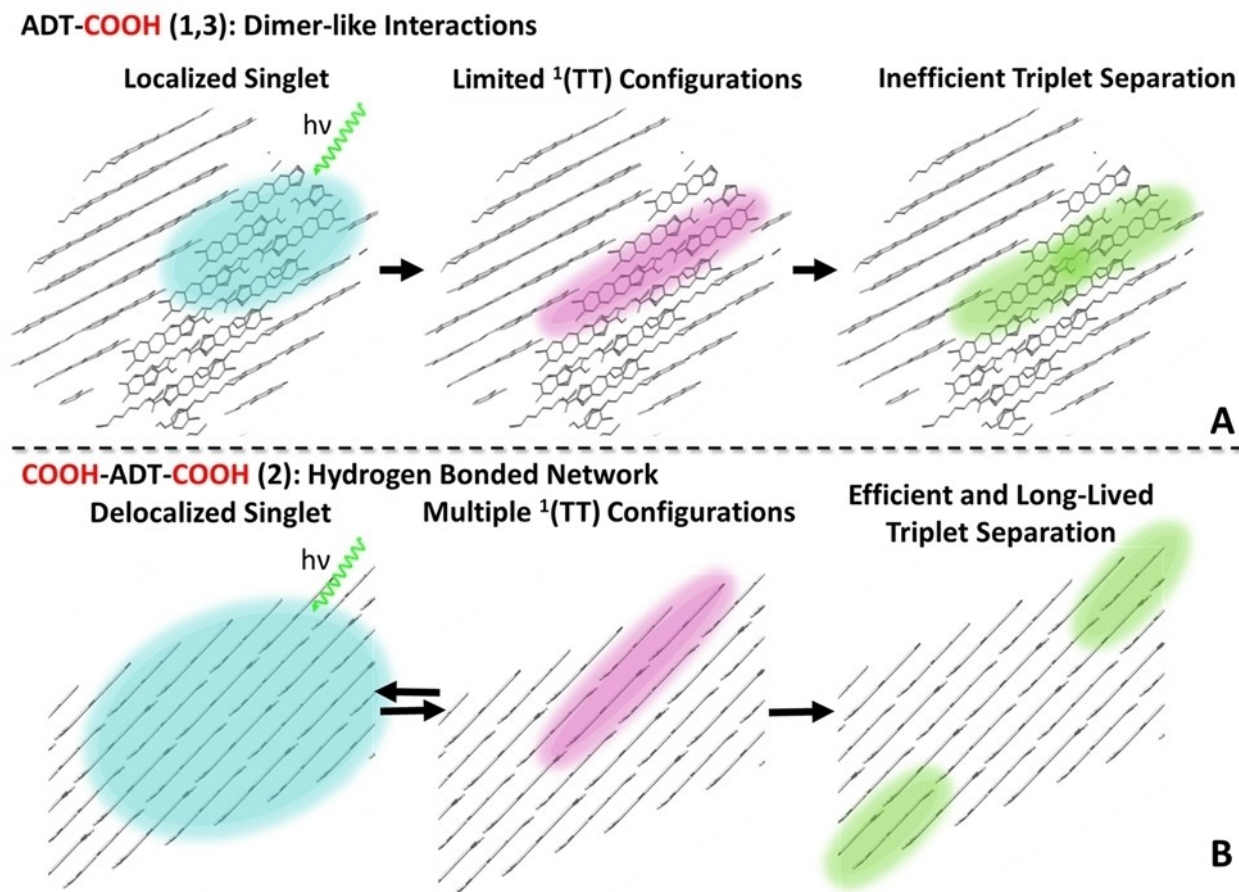
3. Discussion

Despite only small changes to the chemical composition between monoacids (**1**, **3**) and the diacid (**2**), we see dramatic differences in SF behavior between their respective thin films. In contrast, the differences between films of **1** and **3**, which are distinguished by changes in silyl groups, are more subtle. Regardless of a significant increase in crystallinity after solvent vapor annealing a thin film of **3**, the absorption spectrum does not undergo substantial changes, and the SF dynamics are not significantly altered. Solvent vapor annealing of the diacid, however, only slightly increases the crystallinity, yet the contribution of ultrafast SF and the rate of slower SF are both enhanced.

The differences in triplet generation are most obvious at very early pump-probe delays (~200 fs) and long pump-probe delays (1–100 s ns). In the monoacids (**1** and **3**), the spectra indicate no triplet generation occurs within our instrument response (< 200 fs) and we observe a mostly pure singlet spectrum in both the visible and NIR at our earliest pump-probe delay. Triplet signatures grow within 100 ps, but decay quickly with lifetimes of less than 5 ns. In the diacid (**2**), correlated triplet pair and triplet signatures are present at our first observation point followed by a slow decay of separated triplets with lifetimes up to 500 ns.

The appearance of triplet features within 200 fs in the diacid is unusual for other derivatives of anthradithiophenes, which typically behave similarly to the monoacids.[6] The transient behavior and the differences in the steady state absorption spectra suggest that the molecules in the deposited diacid are oriented in a way that promotes ultrafast formation of the correlated triplet pair. The presence of singlet and triplet features in the visible at our early observation time points suggests a quasi-equilibrium between S_1 and $^1(TT)$. On the 10 ps–100 ps time scale, this equilibrium shifts away from S_1 and towards $^1(TT)$, as the channel leading to $T_1 + T_1$ is opened by triplet migration.

The lifetime of free triplets is another indicator of the change in long-range order between monoacids and diacids, suggesting that alteration of $E(2T_1)$ relative to $E(S_1)$ due to extended conjugation introduced by carboxylic acid functionalization is not enough to explain the SF dynamics in these films. The monoacid triplet lifetime is short ($\tau < 5$ ns, Table S4) despite relatively high crystallinity, whereas the diacid triplet lifetime ranges from 150 ns–600 ns (Table S4) and is improved upon annealing. Based on the crystal structure of **3** (Scheme 2A), the hydrogen bonding motif in the monoacid limits strong interactions to at most a few molecules, hindering the efficacy of triplet spatial separation. A two-order of magnitude change in triplet lifetime upon functionalizing both sides of the molecule with carboxylic acids suggests the creation of extended networks of hydrogen bonding on either side of the ADT for **2**, as illustrated in Scheme 2B. In these hydrogen bonded networks, free triplets can migrate quickly to spatially separate more effectively than in the monoacid films.

Inspecting the intermolecular situation in more detail, the large slippage distance in the brickwork crystal structure of each film leaves only the thiophene rings with significant π orbital overlap, which might be a reasonably good juxtaposition for a dimer with slight SF endothermicity, according to simulations of tetracene by Buchanan et al.[8] However, the terminal hydrogens on one thiophene ring for **1** and **3** prevent formation of an extended 3D brickwork pattern, and instead the slip-stacked molecules persist for only four units and subsequently become isolated from nearby brickwork stacks by the TIBS groups (Scheme 2A, side view). The absorption spectrum of **1** exhibits clear signs of coupling that would be expected from the slip-stacked molecular clusters. The expectation from these observations would be reasonably fast SF if the singlet/triplet energy

ChemPhotoChem

Articles
doi.org/10.1002/cptc.202000168

Chemistry Europe
European Chemical
Societies Publishing

Scheme 2. Illustration of singlet fission behavior after photoexcitation of: A) monoacids (**1**, **3**), and B) diacids (**2**).

balance is favorable (i.e., approximately isothermic), but little assistance from delocalization if the balance is endothermic because extended networks cannot form regardless of improved overall crystallinity. The film of **3** is apparently even more unfavorably coupled and in a worse situation than **1**, as judged by the minimal change in absorption spectrum between solution and thin film,[19] weak transient absorption of triplets, and the lack of significant delayed fluorescence. Furthermore, solvent annealing improves the overall crystallinity but induces no change in excited state dynamics. The crystal structure of **3** could not be obtained to confirm the relative intermolecular dispositions.[19] The lack of channels for long-range triplet separation in **1** and **3** can also be cast in terms of entropy if isolated $T_1 + T_1$ configurations are considered the final state. If S_1 and $^1(TT)$ are in quasi-equilibrium, no additional driving force from increased entropy for forcing population toward $T_1 + T_1$ will leave the equilibrium favoring S_1.[11] Thus, the spectral features and lifetimes retain much of their S_1 character and exhibit minimal dependences on temperature. In contrast, the temperature dependence for films of **2** is characterized by an increasingly incomplete transition to independent triplets as temperature is lowered from room temperature (Figure S8,

S12), indicating a thermally activated triplet hopping process. The degree of thermal activation is apparently reduced upon solvent vapor annealing (Figure S9), suggesting that grain boundaries and/or defects are at least partially responsible for the activation barrier for triplet pair separation.

The additional carboxylic acid in **2** facilitates the formation of hydrogen bonded networks that are not interrupted on relevant length scales, leading to a structure that maintains a similar thiophene π-stacked motif that persists over the entire crystal (Scheme 2B). Despite being unable to obtain a crystal structure for **2**, we use the determined crystal structure of **1** and structures of known dicarboxylic acids (e.g. terephthalic acid)[14g,15] to postulate that the carboxylic acid groups of the diacid form cyclic hydrogen bonds[14e,f] (Scheme 2) that drive the local and long-range orientation in thin films. The steady state absorption spectrum of **2** clearly demonstrates strong coupling, and the change in dynamics with improved crystallinity points toward an advantage for phases with long-range ordering. The XRD pattern of **2** shows crystallinity when initially deposited, but a substantial increase in crystallinity after solvent vapor annealing points to some tendency toward

ChemPhotoChem

Articles
doi.org/10.1002/cptc.202000168

Chemistry
Europe
European Chemical
Societies Publishing

kinetically favored disordered phases in as-cast films. Although the size of crystallites is likely much larger than the delocalization length of the singlet, annealing to improve crystallinity could have two effects: (1) it may reduce the influence of grain boundaries, where localization can occur, on the rate of triplet pair separation, or (2) it may reduce the distance needed for photoexcited singlets to move from disordered to crystalline regions to undergo SF. The decreasing time constant for independent triplet growth from 358 ps to 150 ps could be an indicator of either of these processes and since both depends on triplet hopping, the temperature dependence cannot differentiate between them. Future work on films with controlled grain sizes or single crystals could elucidate the situation. TCSPC decays confirm the notion that delayed fluorescence, defined as singlet-like emission that persists beyond the solution fluorescence lifetime, accompanies triplet formation in films **1** and **2**, but is undetectable in the film of **3** that has the weakest signature of triplet formation in TA. The amplitudes of the delayed component are incommensurate with relative long-lived triplet amplitudes from TA for **1** and **2**; however, the delayed fluorescence efficiency may be related to the increased degree of long-range ordering for **2** that enables efficient triplet migration away from the generation site and toward interaction with nonradiative trap centers. Increase in delayed fluorescence intensity upon solvent vapor annealing (Figure S15) may indicate that improved crystallinity leads to a reduction in such trap sites. For **1**, the relative localization of excitations due to the disrupted brickwork pattern leads to only a small amplitude of long-lived triplets ($<10\%$ of total as judged by Figure 5A), yet a larger relative portion of delayed fluorescence than **2** (Figure 5A), possibly due to weaker competition from nonradiative triplet decay.

4. Conclusion

Minor changes in the molecular structure of carboxylic acid substituted anthradithiophene from a monoacid to a diacid lead to significant deviations in the singlet fission dynamics. When deposited into a thin film, the TIPS monoacid **3** is amorphous and when solvent vapor annealed, though crystalline, is limited to dimer-like interactions causing primarily pairwise coupling and slow, inefficient SF. Side group substitution slightly improves the initial crystallinity and the efficiency of SF in the TIBS monoacid, **1**, but only in the diacid is ultrafast triplet pair formation observed and further enhanced after solvent vapor annealing. A temperature dependence in the diacid that is not observed in the monoacid suggests a mechanism that involves activated triplet hopping and an effective entropic contribution arising from the large singlet exciton delocalization radius in the extended brickwork crystal structure. This study demonstrates the potential for hydrogen-bonding driven crystallinity in thin films to increase intermolecular coupling and decrease SF time scales such that a free triplet yield approaching 200% could be found without a strongly

exothermic situation. Further, the ultrafast formation of triplets could facilitate their use at interfaces (i.e., for photochemistry or catalysis) where fast processes involving the singlet are competitive with the utilization of triplets.

Experimental Section

Synthesis

The ADT monocarboxylic acids were prepared by deprotonation of the corresponding ADTs with LDA at low temperature, followed by quenching with carbon dioxide (as detailed in the Supporting Information). Dicarboxylic acid **2** was synthesized as previously reported.[20]

Crystal Structure Determination

X-ray diffraction data were collected at 90.0(2) K on a Bruker-Nonius X8 Proteum diffractometer with graded-multilayer focused CuK(alpha) X-rays. Raw data were integrated, scaled, merged and corrected for Lorentz-polarization effects using the APEX2 package.[21] Corrections for absorption were applied using SADABS.[22] The structure was solved by direct methods (SHELXS)[23] and refined against $F2$ by weighted full-matrix least-squares (SHELXL).[24] Hydrogen atoms were found in difference maps but subsequently placed at calculated positions and refined using a riding model. Non-hydrogen atoms were refined with anisotropic displacement parameters. The final structure model was checked using an R-tensor[25] and by Platon/checkCIF.[26] Atomic scattering factors were taken from the International Tables for Crystallography.[27]

Sample Preparation

For solution studies, compounds were dissolved in THF in a nitrogen glovebox and sealed in a 1 mm cuvette. Thin films of **1**-**3** were deposited on glass through a dropcast method from a saturated THF solution. Solvent vapor annealing was performed with the sample placed in the presence of THF vapor for 3 days. For transient absorption, the films were placed in a sealed chamber in a glovebox to prevent detrimental effects from the presence of oxygen during laser illumination. For temperature studies, the thin films were mounted in an LN_2 cryostat with measurements performed under vacuum at room temperature and 77 K. Triplet sensitization studies were performed in solution using anthracene in THF solution photoexcited at 361 nm or in a thin film configuration using copper phthalocyanine photoexcited at 740 nm in an N_2 atmosphere.

UV-Visible Absorption Spectroscopy

A UV-Visible-NIR absorption spectrophotometer (Agilent Technologies, model 8453 A) was used to collect steady state absorption spectra. An air blank was used to correct the baseline.

X-Ray Diffraction

A Rigaku DMAX 2500 diffractometer with Cu K_α radiation was used to measure intensity as a function of 2θ angle (5–30°).

Time-Resolved Photoluminescence

For the multiplex time-resolved fluorescence experiment, a streak camera (Hamamatsu 300–900 nm, C10910-04) was used to detect time-resolved spectra. The instrument response function is approximately 100 ps. An NKT supercontinuum fiber laser (SuperK EXU-6-PP) operating at 2 MHz and 515 nm was used as the excitation source.

Time-Correlated Single Photon Counting

Time-correlated single photon counting (TCSPC) was used to monitor delayed fluorescence. A PicoHarp 300 TCSPC module was utilized along with a pulsed diode laser (PDL 800-B, $\lambda_{pump} = 450$ nm) as the excitation source.

Femtosecond Transient Absorption Spectroscopy

Ultrafast transient absorption measurements were performed using a Coherent Libra Ti:Sapphire laser with an 800 nm output (150 fs pulse width) at 1 kHz. The 500 nm and 625 nm pump pulses were generated using a TOPAS-C optical parametric amplifier. Pulse energies are 35 nJ/pulse unless otherwise stated. White light probe pulses were generated by focusing a small amount of the 800 nm output into a thin sapphire window for visible ($\lambda_{probe} = 440$–800 nm) or a thick sapphire window for NIR measurements ($\lambda_{probe} = 750$–1600 nm). The probe was delayed relative to the pump using a mechanical delay stage and pump and probe were focused and spatially overlapped at the sample. A small amount of the probe was picked off before the sample for a reference to reduce signal-to-noise to 0.1 mOD. Data were chirp corrected and analyzed using SurfaceXplorer software from Ultrafast Systems. Global analysis was performed using Glotaran v 1.5.1.

Nanosecond-Microsecond (1 ns–400 μs) Transient Absorption Spectroscopy

In nanosecond-microsecond transient absorption measurements (EOS, Ultrafast Systems), the same pump pulse was used as in the fsTA. The probe pulse originated from continuum generation in a diode-laser pumped photonic crystal fiber and electronically delayed relative to the pump pulse using a digital delay generator.

Conflict of Interest

The authors declare no conflict of interest.

[1] M. B. Smith, J. Michl, *Chem. Rev.* **2010**, *110*, 6891–6936.

[2] M. B. Smith, J. Michl, *Annu. Rev. Phys. Chem.* **2013**, *64*, 361–386.

[3] a) M. K. Gish, N. A. Pace, G. Rumbles, J. C. Johnson, *J. Phys. Chem. C* **2019**, *123*, 3923–3934; b) N. A. Pace, D. H. Arias, D. B. Granger, S. Christensen, J. E. Anthony, J. C. Johnson, *Chem. Sci.* **2018**, *9*, 3004–3013.

[4] a) J. C. Dean, R. Zhang, R. K. Hallani, R. D. Pensack, S. N. Sanders, D. G. Oblinsky, S. R. Parkin, L. M. Campos, J. E. Anthony, G. D. Scholes, *Phys. Chem. Chem. Phys.* **2017**, *19*, 23162–23175; b) C. K. Yong, A. J. Musser, S. L. Bayliss, S. Lukman, H. Tamura, O. Bubnova, R. K. Hallani, A. Meneau, R. Resel, M. Maruyama, S. Hotta, L. M. Herz, D. Beljonne, J. E. Anthony, J. Clark, H. Sirringhaus, *Nat. Commun.* **2017**, *8*, 15953.

[5] Y. D. Zhang, Y. Wu, Y. Xu, Q. Wang, K. Liu, J. W. Chen, J. J. Cao, C. Zhang, H. Fu, H. L. Zhang, *J. Am. Chem. Soc.* **2016**, *138*, 6739–6745.

[6] a) R. D. Pensack, A. J. Tilley, C. Grieco, G. E. Purdum, E. E. Ostroumov, D. B. Granger, D. G. Oblinsky, J. C. Dean, G. S. Doucette, J. B. Asbury, Y. L. Loo, D. S. Seferos, J. E. Anthony, G. D. Scholes, *Chem. Sci.* **2018**, *9*, 6240–6259; b) D. H. Arias, J. L. Ryerson, J. D. Cook, N. H. Damrauer, J. C. Johnson, *Chem. Sci.* **2016**, *7*, 1185–1191; c) A. K. Le, J. A. Bender, D. H. Arias, D. E. Cotton, J. C. Johnson, S. T. Roberts, *J. Am. Chem. Soc.* **2018**, *140*, 814–826; d) R. D. Pensack, A. J. Tilley, S. R. Parkin, T. S. Lee, M. M. Payne, D. Gao, A. A. Jahnke, D. G. Oblinsky, P. F. Li, J. E. Anthony, D. S. Seferos, G. D. Scholes, *J. Am. Chem. Soc.* **2015**, *137*, 6790–6803.

[7] a) L. Wang, Y. Olivier, O. V. Prezhdo, D. Beljonne, *J. Phys. Chem. Lett.* **2014**, *5*, 3345–3353; b) S. R. Yost, J. Lee, M. W. Wilson, T. Wu, D. P. McMahon, R. R. Parkhurst, N. J. Thompson, D. N. Congreve, A. Rao, K. Johnson, M. Y. Sfeir, M. G. Bawendi, T. M. Swager, R. H. Friend, M. A. Baldo, T. Van Voorhis, *Nat. Chem.* **2014**, *6*, 492–497; c) P. M. Zimmerman, F. Bell, D. Casanova, M. Head-Gordon, *J. Am. Chem. Soc.* **2011**, *133*, 19944–19952.

[8] E. A. Buchanan, Z. Havlas, J. Michl, *Bull. Chem. Soc. Jpn.* **2019**, *92*, 1960–1971.

[9] S. T. Roberts, R. E. McAnally, J. N. Mastron, D. H. Webber, M. T. Whited, R. L. Brutchey, M. E. Thompson, S. E. Bradforth, *J. Am. Chem. Soc.* **2012**, *134*, 6388–6400.

[10] a) W. L. Chan, M. Ligges, X. Y. Zhu, *Nat. Chem.* **2012**, *4*, 840–845; b) A. B. Kolomeisky, X. Feng, A. I. Krylov, *J. Phys. Chem. C* **2014**, *118*, 5188–5195.

[11] N. Korovina, C. H. Chang, J. C. Johnson, *Nat. Chem.* **2020**, *12*, 391–398.

[12] a) A. Camposeo, D. B. Granger, S. R. Parkin, D. Altamura, C. Giannini, J. E. Anthony, D. Pisignano, *Chem. Mater.* **2019**, *31*, 1775–1783; b) J. E. Anthony, *Chem. Rev.* **2006**, *106*, 5028–5048.

[13] a) G. B. Piland, C. J. Bardeen, *J. Phys. Chem. Lett.* **2015**, *6*, 1841–1846; b) P. E. Hartnett, E. A. Margulies, C. M. Mauck, S. A. Miller, Y. Wu, Y. L. Wu, T. J. Marks, M. R. Wasielewski, *J. Phys. Chem. B* **2016**, *120*, 1357–1366.

[14] a) A. M. Beatty, *Coord. Chem. Rev.* **2003**, *246*, 131–143; b) N. Shan, A. D. Bond, W. Jones, *Cryst. Eng.* **2002**, *5*, 9–24; c) E. Batchelor, J. Klinowski, W. Jones, *J. Mater. Chem.* **2000**, *10*, 839–848; d) M. L. Cheney, D. R. Weyna, N. Shan, M. Hanna, L. Wojtas, M. J. Zaworotko, *Cryst. Growth Des.* **2010**, *10*, 4401–4413; e) J. Dong, Y. Ozaki, K. Nakashima, *Macromolecules* **1997**, *30*, 1111–1117; f) L. Sun, L. J. Kepley, R. M. Crooks, *Langmuir* **1992**, *8*, 2101–2103; g) G. R. Desiraju, *J. Mol. Struct.* **2003**, *656*, 5–15.
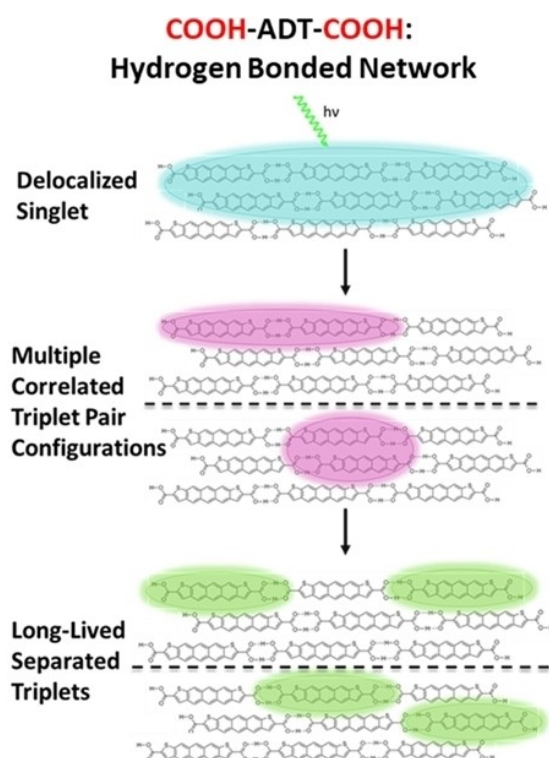
ChemPhotoChem

Articles
doi.org/10.1002/cptc.202000168

Chemistry Europe
European Chemical
Societies Publishing

[15] M. Sledz, J. Janczak, R. Kubiak, *J. Mol. Struct.* **2001**, *595*, 77–82.

[16] S. H. Lim, T. G. Bjorklund, F. C. Spano, C. J. Bardeen, *Phys. Rev. Lett.* **2004**, *92*, 107402.

[17] K. D. M. Harris, E. Y. Cheung, *Chem. Soc. Rev.* **2004**, *33*, 526–538.

[18] N. A. Pace, N. V. Korovina, T. T. Clikeman, S. Holliday, D. B. Granger, G. M. Carroll, S. U. Nanayakkara, J. E. Anthony, I. McCulloch, S. H. Strauss, O. V. Boltalina, J. C. Johnson, G. Rumbles, O. G. Reid, *Nat. Chem.* **2020**, *12*, 63–70.

[19] J. C. Sorli, Q. Ai, D. B. Granger, K. Gu, S. Parkin, K. Jarolimek, N. Telesz, J. E. Anthony, C. Risko, Y. L. Loo, *Chem. Mater.* **2019**, *31*, 6615–6623.

[20] Z. Li, Y. F. Lim, J. B. Kim, S. R. Parkin, Y. L. Loo, G. G. Malliaras, J. E. Anthony, *Chem. Commun. (Camb.)* **2011**, *47*, 7617–7619.

[21] Bruker, *Bruker-AXS* **2006**, *Madison, WI. USA*.

[22] L. Krause, R. Herbst-Irmer, G. M. Sheldrick, D. Stalke, *J. Appl. Crystallogr.* **2015**, *48*, 3–10.

[23] G. M. Sheldrick, *Acta Crystallogr. Sect. A* **2008**, *64*, 112–122.

[24] G. M. Sheldrick, *Acta Crystallogr. A Found Adv.* **2015**, *71*, 3–8.

[25] S. Parkin, *Acta Crystallogr. Sect. A* **2000**, *56 (Pt 2)*, 157–162.

[26] A. L. Spek, *Acta Crystallogr. D Biol Crystallogr.* **2009**, *65*, 148–155.

[27] E. A. J. C. Wilson, *International Tables for Crystallography, vol. C: Mathematical, Chemical, and Physical Tables*, Kluwer Academic Publishers, Dordrecht, Holland, **1992**.

ARTICLES

Dr. M. K. Gish, Dr. K. J. Thorley,
Dr. S. R. Parkin, Dr. J. E. Anthony,
Dr. J. C. Johnson*

Hydrogen Bonding Optimizes Singlet Fission in Carboxylic Acid Functionalized Anthradithiophene Films

Building bridges: Carboxylic acid functionalization of anthradithiophenes (ADT) affects ordering in thin films via hydrogen bonding. The extended network of hydrogen bonds in the diacid ADT allows for fast and efficient triplet formation and long-lived, effective triplet separation. The monoacid ADT has limited interactions, which leads to fast triplet decay.